Low frequency magnetic variations at the high-β Earth bow shock

Anatoli A. Petrukovich[1], Olga M. Chugunova[1], and Pavel I. Shustov[1]

[1]Space Research Institute of Russian Academy of Sciences, Moscow, Russia

Correspondence: A.A.Petrukovich (a.petrukovich@cosmos.ru)

Abstract. Observations of Earth's bow shock during high β (ratio of thermal to magnetic pressure) solar wind streams are rare. However such shocks are ubiquitous in astrophysical plasmas. Typical solar wind parameters related with high β (here $\beta > 10$) are: low speed, high density and very low interplanetary magnetic field 1–2 nT. These conditions are usually quite transient and need to be verified immediately upstream of the observed shock crossings. In this report, three characteristic crossings by the Cluster project (out of 22 found) are studied with multipoint analysis allowing us to determine spatial scales. The main magnetic field and density spatial scale of about a couple of hundred km generally corresponds to the increased proton convective gyroradius. Observed magnetic variations is different from that for supercritical shocks with $\beta \sim 1$. Dominate magnetic variations in the shock transition have amplitudes much larger than the background field and frequency of ~ 0.3–0.5 Hz (in some events — 1–2 Hz). The wave polarization has no stable phase and is closer to linear, complicating determination of the wave propagation direction. Spatial scales (wavelengths) of variations are within several tens to couple hundred km.

Copyright statement. TEXT

1 Introduction

Shocks are the primary dissipation mechanism in space plasmas with supersonic flows (Sagdeev, 1966; Kennel et al., 1985; Krasnoselskikh et al., 2013). A new branch of plasma science, theory of collisionless shocks, appeared in the sixties, in response to new space observations. The solar wind forms bow shocks at planets and comets, as well as the termination shock at the heliospheric interface. Interplanetary shocks develop inside the heliosphere after solar eruptions, when large-scale transient structures propagate relative to the regular solar wind flow. In more distant space, shocks are associated with supernova explosions, stellar winds, collisions of galaxy clusters and are believed to have a leading role in the acceleration of cosmic rays (Axford et al., 1977; Krymskii, 1977). The physics of space shocks was reviewed in AGU Geophysical Monographs, volumes 34 and 35 (1985). The Earth bow shock has been most thoroughly studied and is the main source of our in-situ knowledge of collisionless shock structure and dynamics.

Electromagnetic fields and waves in collisionless plasma shocks are of primary importance. Due to presence of the magnetic field, a wide variety of shock types exists with quite differing structure (Kennel et al., 1985). The magnetic field vector is a key parameter in the Rankine-Hugoniout equations, defining the relation between upstream and downstream conditions. In the

absence of collisions, kinetic mechanisms of field-particle interactions are responsible for dissipation and particle acceleration (Sagdeev, 1966; Krasnoselskikh et al., 2013). With quasi-perpendicular shock geometry (when the angle between the shock normal and the upstream magnetic field is closer to 90°) ions cannot escape upstream and relatively sharp shock transition forms with the overall width of several thousand km. In a quasi-parallel geometry (the angle is closer to 0°) ions easily
5 escape upstream along magnetic field and shock transition smears to the scales around several Earth radii (Scudder et al., 1986; Burgess et al., 2005). Oblique shocks (angles around 45°) are in a sense intermediate in properties, when ions partially are capable to escape upstream, but generally have rather spatially localized transition similar to quasi-perpendicular ones.

 Besides this large-scale magnetic field structure, also of interest at the Earth's bow shock are relatively low frequency magnetic variations (from one tenth to few Hz) with visually maximal amplitudes, which actually form the primary shock front
10 structure and dissipate ions. For example, in a supercritical quasi-perpendicular shock, the oblique whistler waves near the lower-hybrid frequency ($\sim$5 Hz) form the magnetic ramp via the non-linear steepening and decay cycle (Krasnoselskikh et al., 2002, and references therein). In the several studies the wavelength of these waves and the scale of shock ramp were determined to be around 10-s of km and oscillations were in fact identified as whistlers (Petrukovich et al., 1998; Walker et al., 2004; Hobara et al., 2010; Schwartz et al., 2011; Dimmock et al., 2013; Krasnoselskikh et al., 2013). Cyclic shock reformation is
15 typical also for quasi-parallel shocks with substructures known as SLAMS and oblique shocks (Lefebvre et al., 2009). Specifics of the plasma wave mode driving the front reformation depends of local plasma parameters, Mach number, etc. Immediately downstream of the shock front plasma waves at frequencies below that of ion cyclotron motion were attributed to mirror, ion cyclotron, intermediate modes (e.g., Balikhin et al., 1997; Czaykowska et al., 2001). Yet one more issue of interest is electron heating. It requires sufficiently small scale variations for non-adiabatic acceleration and subsequent isotropisation
20 (Balikhin et al., 1993; Vasko et al., 2018).

 Of interest to several astrophysical applications are shocks in a weak magnetic field environment (high-β shocks), common in interstellar and intergalaxy space (e.g., Markevitch and Vikhlinin, 2007; Donnert et al., 2018). β is a dimensionless parameter, the ratio of plasma thermal to magnetic energy density. For low background magnetic fields, shock-associated variations may be also considered as kind of 'magnetic field amplification', increasingly important for particle heating. Unfortunately,
25 observations of high β shocks near Earth are quite rare, since the solar wind plasma usually has $\beta \sim 1$.

 In our study we take $\beta > 10$ as threshold of high β, this choice is explained further below. Very few investigations of high-β shocks have been published. Coroniti (1970) in a theoretical study suggested the Alfvén mode to dominate downstream of such a shock. Formisano et al. (1975) presented three cases of OGO-5 spacecraft observations with β equal to 8, 170, 49. The general structure of these crossings was discussed. Large magnetic field excursions up to 20 times larger than the upstream
30 interplanetary magnetic field (IMF) were reported. The presence of some transient 'precursor activations' upstream of the main transitions was interpreted as a sign of principal nonstationarity of a shock structure. It was concluded that despite formal high β, the magnetic field should not be ignored in theory studies of shock structure. Winterhalter and Kivelson (1988) stated that shock appearance with high-amplitude magnetic variations is typical for the cases with higher β. Specific examples of interest to our study were not shown. Farris et al. (1992) investigated one shock with β equal to 18, checking the validity of Rankine-
35 Hugoniot conditions and also mentioning high-amplitude magnetic variations. However, neither of these studies considered in

detail these variations at the shock transition zone. Finally, we also note, that in some, rather numerous, investigations moderate $\beta \geq 1$ was termed as "high-β" regime (e.g., $\beta = 2.4$ in Scudder et al., 1986).

We perform an extended experimental study of high-β bow shocks, with a first, to the best of our knowledge, multi-point analysis of dominating low-frequency magnetic varations at high-β shock transition using observations of Cluster project.
5   To access possible solar wind variability we use also ACE and Wind final Earth-shifted data from OMNI-2 archive. Though such solar wind statistics are generally known (review in Wilson et al., 2018), some issues relevant to shock identification and analysis are still worth addressing. All vectors in this paper are in GSE frame of reference.

2   Solar wind statistics and details of search procedure

We use 1-hour OMNI-2 data for the period 1995–2017 to determine the occurrence of high β solar wind for our subsequent
10   shock analysis. β values are precalculated in OMNI-2, assuming constant electron temperature (140000 K), He++ fraction (0.05) and He++ temperature (four times larger than proton temperature). The average solar wind β is somewhat large than unity. High β conditions are unevenly distributed across solar cycles (Fig. 1), being more frequent at the solar minima 1996–1997 and 2007–2009. For the threshold $\beta > 10$ there are 50–500 hours per year, while for $\beta > 20$, the number is about 3–5 times smaller.
15   Figure 2 shows distributions of magnetic field magnitude, solar wind speed, density and total static pressure for the full dataset of one-hour values during 1995–2017 and for the subset $\beta > 10$. High β corresponds to slow, cold and dense solar wind with low magnetic field (ion temperature not shown here). However, the total static (magnetic plus thermal) pressure distribution is similar (Fig. 2b). Thus the high-β events are mostly depressions of magnetic field, compensated (at least on average) by increase of plasma density. The only notable difference of distributions for $\beta > 20$ (Fig. 2a, red line) is more
20   frequent presence of magnetic field $\sim$1 nT, with the average 1.6 nT, while for $\beta > 10$ the average is $\sim$2.2 nT.

More than 50% of events with $\beta > 10$ have one-hour duration (one point in the analysed OMNI variant, not shown here). A sample event is in Fig. 3 (here 1-min OMNI-2 variant is used). There is about one-hour long decrease of magnetic field and density increase, corresponding to $\beta \sim$20. At an occasional depletion of magnetic field below 2 nT, β jumps to about 40–80 for few minutes. Since formation of high β conditions mostly depends on subtle variations of magnetic field magnitude around
25   1–2 nT (note, that β has square dependence on magnetic field), it should be quite sensitive to spatial inhomogeneity of the solar wind and IMF, and, in particular, to differences between those detected at L1 (in OMNI dataset) and actually hitting Earth. Fig. 4 shows comparison of β calculation for Wind and ACE 1-hour data (only for times, when Wind data were used in OMNI). The scatter is indeed large. For this OMNI-2 subset there were 618 1-hour points, with $\beta >$10 either in Wind or ACE data. Only for 196 of them the difference of β at two spacecraft was less than 30%. For more than half of events (318) difference
30   between the spacecraft was larger than 50%.

We formulate several conclusions important for our specific shock analysis. (1). Solar wind intervals with high $\beta =$10–20 are rare, but not extremely rare, and occur mostly during solar minimum. Thus some spacecraft (or the project phases with the specific orbit or spacecraft separation) may almost completely miss such events. (2). Duration of intervals of interest
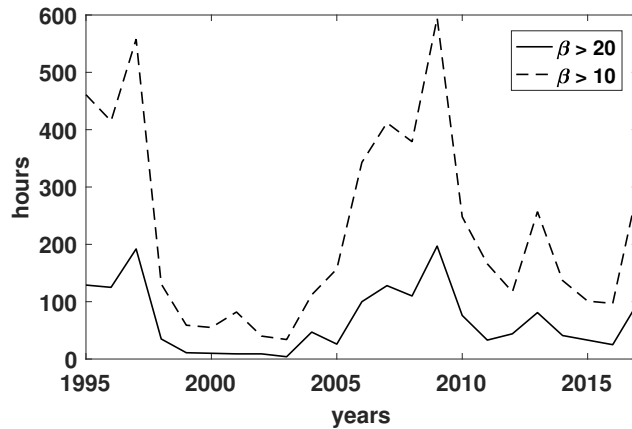
Figure 1. Number of hours with high β with respect to calendar year.

is relatively short, thus selection of shocks with the stable upstream conditions may be not always possible. (3). Very low interplanetary magnetic field, necessary for high-β events, is subject to strong (in relative terms) intrinsic spatial and temporal variability, thus actual β conditions and IMF vector need to be always rechecked with local measurements. This issue is further illustrated with the event selection results below and is elaborated more in Discussion.

5   Since the high-β shocks are rare, it is unreasonable to search for them, rechecking every registered event. It is more practical first to identify the intervals with the suitable conditions of solar wind. The semi-automated algorithm is used to assemble initial statistics of the shock candidates. For each 1-hour point in OMNI with $\beta > 10$, we check for possible spacecraft location within 5 R_E from the model bow shock (Farris et al., 1991). We scanned 1995–2017 observations by all available spacecraft (Geotail, Interball, THEMIS, Cluster). For this initial selection we use orbital data and spin-averaged magnetic field data from
10   CDAWeb archive.

In a case any spacecraft is in the right place, the plots of solar wind, IMF, local magnetic field and plasma parameters are analyzed visually in the 5-hour window around the selected hour. These broad temporal and spatial spans are used to ensure that all possible crossings of a moving bow shock are captured for future analysis. Only events with the clear shock traversals (jumps in magnetic field and ion density) are accepted. Such a manual selection has definite bias to quasi-perpendicular and
15   oblique shocks (which usually have a step-like appearance), but it is considered acceptable for this particular study. The most of these initially selected intervals actually contain no shock crossings.

Discovered particular shock crossings are checked with 1-min OMNI data. Plasma β is often below 10, either because registered shocks are just outside of initially selected hours, or because β varied on a time scale, smaller than an hour. Since a change of β is usually accompanied with the solar wind density change, there is a dynamic pressure change also. The latter
20   drives large-scale shock motion and probability of shock registration by a spacecraft increases. In fact, many shock crossings are registered at a boundary of β change and such events are also discarded, since it is impossible to attribute them to stable upstream plasma conditions.
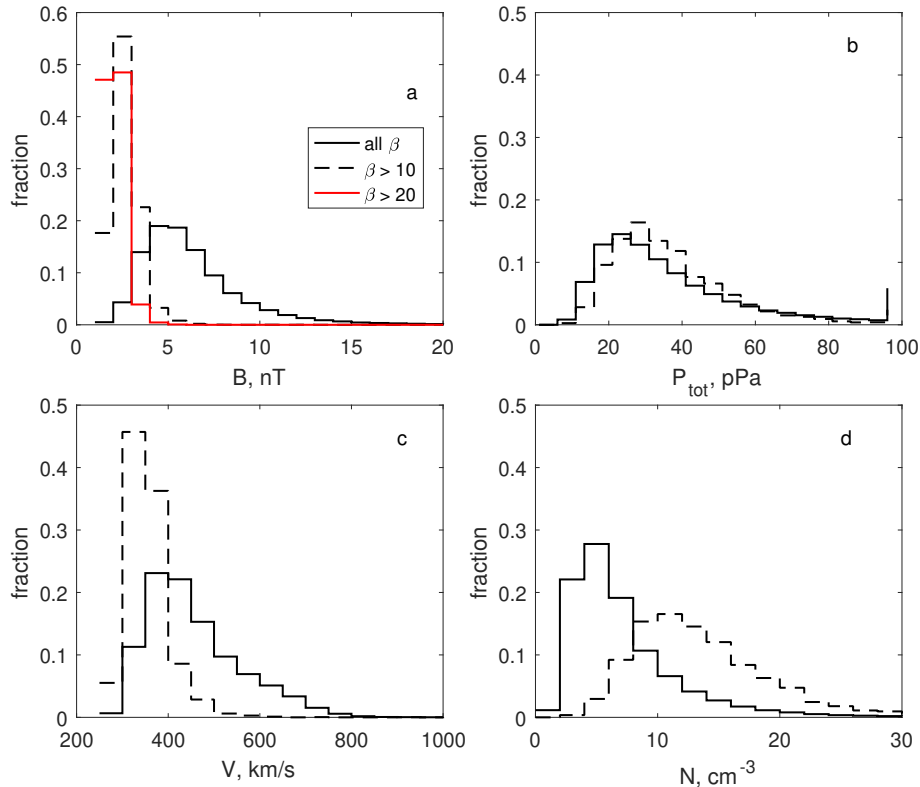
Figure 2. Histograms of solar wind and IMF occurrence for 1995–2017 (solid lines) and for $\beta > 10$ (dashed lines) subset. (a) Total magnetic field (red line corresponds to $\beta > 20$) , (b) total static pressure, (c) solar wind speed, (d) ion density. Red line $\beta > 20$ is not given at other panels, since it is almost identical to $\beta > 10$ one.

This preliminary list contains about a hundred crossings with the average β about 20 (taken as 1-min OMNI value at the moment of shock front crossing). Eleven events occurred with very high $\beta > 40$. The choice of initial threshold $\beta > 10$ (for 1-hour points) was finally justified at this stage, since a variant with initial $\beta > 20$ resulted with the almost empty list. However, all these events still need a more detailed confirmation, in particular, of local high β, stable enough crossing velocity, plasma data availability etc.

For the specific multipoint analysis in this investigation we selected 22 verified Cluster project shock crossings with relatively small spacecraft separation. The full list is in Table S1 in Supplement 1. For the detailed analysis we used full-resolution Cluster FGM magnetic field (here with the sampling ∼20 Hz) (Balogh et al., 2001) and HIA/CODIF ion data (sampling once in 4–12 s, depending on a parameter) (Rème et al., 2001) from Cluster Science Archive. Since HIA/CODIF data may be not fully reliable to provide ion/proton density (and temperature) in solar wind, we additionally use WHISPER instrument electron density data (Décréau et al., 2001).

One event is from 2003, with the Cluster tetrahedron size of about 300 km, while the others are for the later years 2008–2016, when separation only between a pair of Cluster spacecraft C3 and C4 was controlled (30–150 km for our events). This uneven
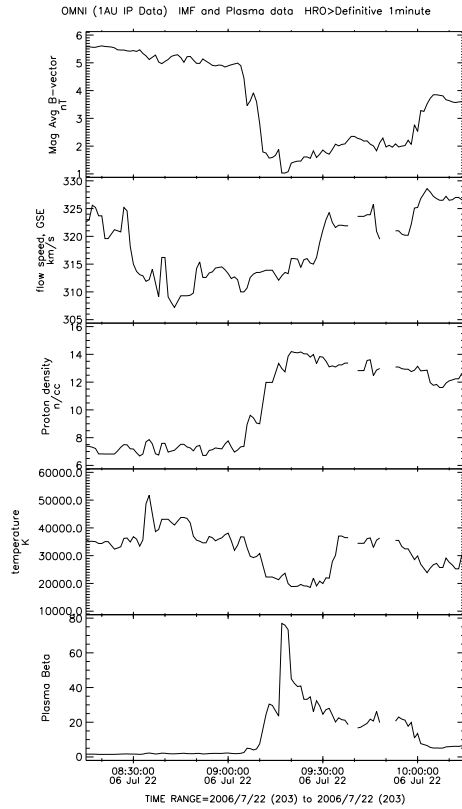
Figure 3. Example of high-β interval. From top to down: magnetic field magnitude, solar wind speed, proton density, proton temperature, plasma β. 1-min OMNI data set used.

annual distribution is a consequence of the solar cycle dependence (Fig. 1). Events are grouped in only 7 days. Specifically, 5 crossings are registered within one hour at December 18, 2011, 4 crossings — within two hours at January 3, 2008, 8 crossings — within two hours at January 4, 2008, 2 crossings — within one hour at February 16, 2012. However not all these adjacent crossings are similar. Three characteristic examples are presented below.

3   Shock examples

3.1   Event 1

The first example is registered on 18 December 2011 (14:36–14:40 UT) by Cluster C3 and C4 with the separation 36 km. The spacecraft orbit is almost parallel to the model shock (Fig. 5). Fig. 6 contains overview of magnetic field and plasma
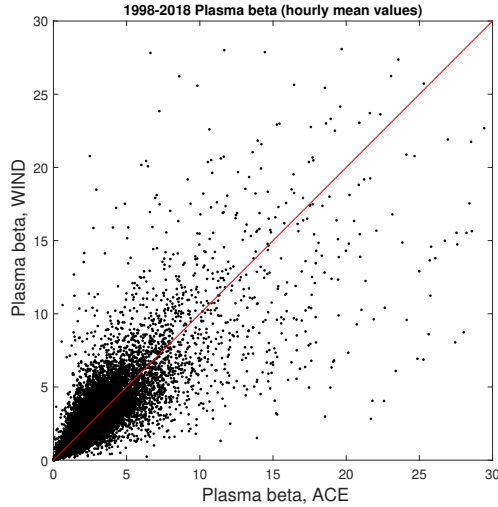
Figure 4. Comparison of Wind and ACE β using 1-hour data. See text for details. Red line is bisector

parameters. Solar wind speed is small ~ 260 km/s, IMF magnitude — 2.5 nT (all characteristics are in Table S1). Alfvén Mach number is ≈ 18, magnetosonic Mach number is ≈ 5, β (according to 1-min OMNI) is 10.8.

The ion (proton) density in solar wind according to Cluster is lower, than that in OMNI. However, the WHISPER electron density is almost the same. The proton perpendicular temperature grows as expected towards downstream, while the parallel temperature peaks just upstream the shock front. We attribute this peak to upstream-moving field-aligned protons. The presence of two populations with the strongly different flow velocity results in the false temperature increase. Thus using local ion data to calculate local β would be unreliable. We confirm β using only local magnetic field , since it is the most variable parameter (in comparison with the plasma density). Solar wind magnetic field measured locally by Cluster is the same as OMNI data (compare two lines in Fig. 6d). OMNI IMF vector direction is $\sim 10^o$ different with the local upstream field taken at 14:40–14:41 UT (not shown here).

The model shock normal angle θ_{Bn} with respect to OMNI (local) IMF is 46° (54°) (using Farris et al. (1991) model). The coplanarity calculation for the shock normal results in θ_{Bn} equal to 42°. Downstream and upstream intervals were taken as 14:36-14:37 UT and 14:40-14:41 UT, respectively. Thus this is quasi-perpendicular or oblique supercritical bow shock with reliably determined geometry. Such crossings for more standard β are well studied (Scudder et al., 1986; Krasnoselskikh et al., 2013; Lefebvre et al., 2009). The compression ratios for magnetic field and plasma density are 3.55 and 3.65 respectively.

The shock transition lasts about 200 seconds (14:37:00–14:40:30 UT) from the first signs of the upstream high-energy ions, which can be observed on the spectrogram in Fig. 6f up to the stable downstream conditions.

The increase in magnetic field magnitude and ion density (shock ramp in a quasi-perpendicular case) is smeared over half a minute (14:37:45-14:38:20 UT). The nominal shock front transition is somewhat arbitrarily placed at 14:37:45 UT (marked by vertical line) at a first extended peak of magnetic field. The magnetic field increase has no regular or step-like form, and

the magnetic magnitude immediately downstream is often down to 5 nT. Thus it is impossible to determine the shock speed, comparing C3 and C4 measurements.

However, Cluster 2, about 6000 km away from the pair C3 and C4, crossed the shock two minutes later (exact values are 6231 km and 124 s between C3 and C2, not shown here). The separation of C3 and C2 along the model normal is 1032 km, the spacecraft pair is elongated along the shock front. The shock speed along the normal is 8.3 km/s outbound. This calculation is not very reliable for two reasons: (1) The spacecraft are mostly separated along the front by about 6000 km and the shock motion may be different in two so different points. (2) The subsequent crossing in the reverse direction occurred less than 10 min later, thus the shock speed might substantially change on a scale of two min (separation between C3 and C2). Nevertheless, one can estimate the spatial scale of the ramp. Duration of 35 s corresponds to 290 km. The convective gyroradius of solar wind proton in IMF is ~1200 km, in the downstream magnetic field is 380 km, while the ion inertial length in solar wind is ~66 km (in these estimates we neglected small shock speed).

We highlight, in Figure 7, the interval with the strongest low-frequency magnetic variations. Frequency spectra are shown in Figure 8. The magnetic profile is dominated by a variation with frequency around 0.3 Hz and amplitude up to 20 nT, more pronounced in B_y. An interval 14:37:27–14:37:47 UT is taken to estimate the wavelength. Since the variation has a clear dominating frequency, it is more convenient to perform time-domain multi-point analysis.

Parameters of magnetic variations, filtered in frequency range 0.1–0.77 Hz, are presented in Table 1. The vector of maximum variance is almost along local magnetic field (B_y component dominates), of minimum variance — along Z. Ratios of eigenvalues are $\lambda_{min}/\lambda_{int} = 0.34$, $\lambda_{int}/\lambda_{max} = 0.58$, and one may assume elliptic polarization. The time shift between magnetic measurements along the maximum variance component, determined with the correlation analysis, is 0.13 s. This value is rather reliably calculated, since it is 2–3 times larger than the sampling interval. This shift is also persistently visible in the relevant interval at Fig.7a,b. The spacecraft separation along the minimum variance direction is 10 km and the resulting wavelength estimate is ~250 km.

However, the hodograph of magnetic field rotation (Fig. 9) shows that the polarization actually might be linear with the maximum variance direction changing every several periods (two variants are shown by red lines). In such a case the propagation direction cannot be defined with the variance analysis. For compressive low frequency MHD waves the propagation direction can be determined with the coplanarity approach (Hubert et al., 1998). Namely, the maximum variance direction, the magnetic field direction and the wavevector should be in the same plane. In this case, the angle between the maximum variance direction and the local magnetic field is rather small (only 12°) and coplanarity calculation would be unrealiable.

We also estimate the span of principally possible wavelengths. The maximal one is ~900 km, obtained taking full spacecraft separation 36 km. Both estimates (250 and 900 km) are approximately equal or larger than local ion gyroradius (330 km, introduced above). The Doppler shift is 0.04–0.58 Hz, depending on wavelength and taken local proton velocity value (full 146 km/s or its projection to the minimum variance eigenvector 41 km/s).

Finally we note the oscillations with higher frequency about 1 Hz and smaller amplitude of couple nT, which are best observable in B_z component (Fig. 7c and Fig. 8). The eigenvalue ratios (after filtering the frequency range 0.7–10 Hz) are
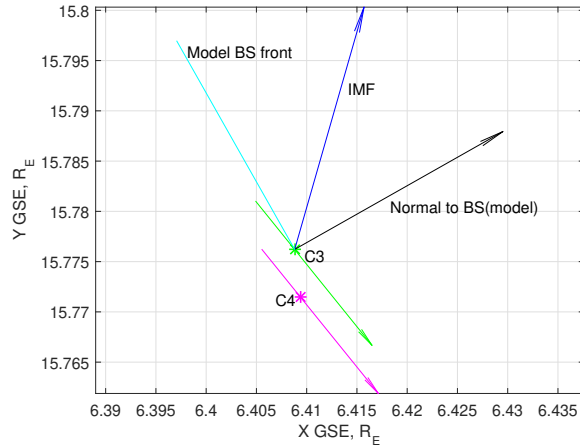
Figure 5. Spacecraft orbit and model shock for shock 12 December 2011.

$\lambda_{min}/\lambda_{int} = 0.68$, $\lambda_{int}/\lambda_{max} = 0.49$, thus reliable determination of any wave proper direction is definitely not possible. Oscillations are quite different at two spacecraft and the multipoint analysis also proved to be not possible.

3.2 Event 2

A shock from January 4th, 2008 (16:00–16:04 UT) was registered with Cluster C3 and C4 separation about 40 km. General event parameters are in Table S1, overview of plasma and magnetic field parameters is in Fig.S1 in Supplement. The detailed wave activity at the front is presented in Fig. 10. Solar wind parameters and general crossing structure are very similar to that for Event 1. Solar wind speed is small ∼315 km/s, IMF magnitude — 2.4 nT. Alfvén Mach number is ≈23, magnetosonic Mach number is ≈7, β (according to 1-min OMNI) is 12.2. Solar wind magnetic field measured locally by Cluster is the same as OMNI data (compare two lines in Fig. S1d), therefore OMNI β value is confirmed. All variants for θ_{Bn} give ∼40°.

The transition lasts about 2 minutes (16:00:50–16:02:50 UT) from the first signs of upstream high-energy ions and ion velocity change to the stable downstream conditions (Fig. S1f). The jump in magnetic field magnitude and ion density is smeared over half a minute 16:01:30-16:02:00 UT, and is wavy rather than step-like, downstream magnetic magnitude is often as small as 2–5 nT. The nominal shock front transition is somewhat arbitrarily placed at 16:01:35 UT at a first extended peak of magnetic field.

In general, this ramp transition is a slow ≈30 s long simultaneous increase of magnetic field and ion density, visually similar to Event 1. Characteristic plasma scales for this Event 2 are almost equal to the values for Event 1. Comparing with
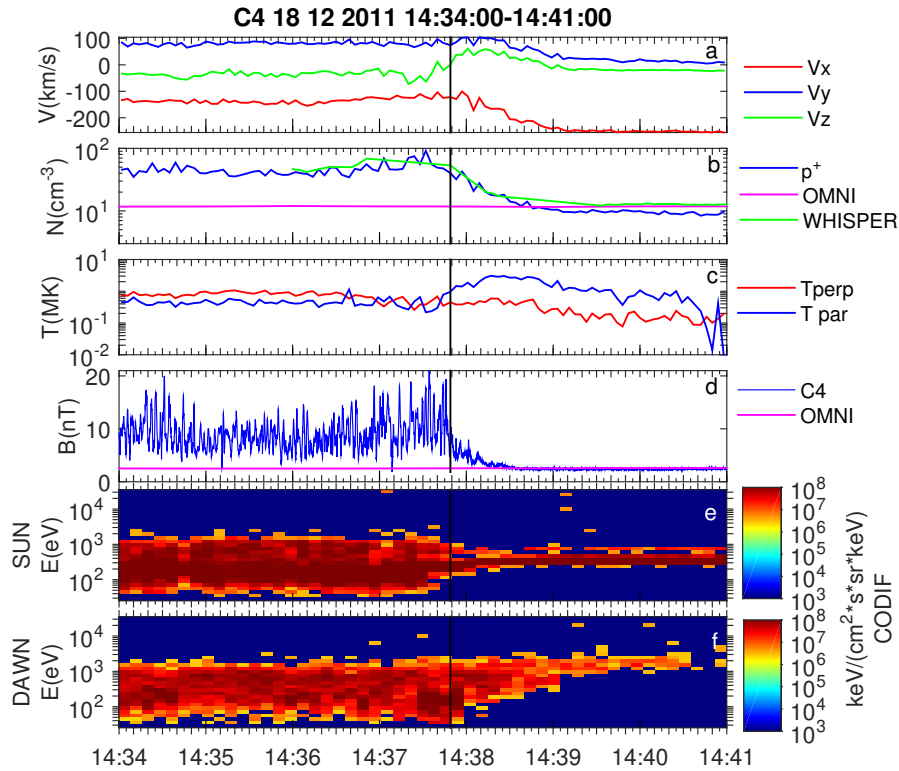
Figure 6. Overview of C4 magnetic and plasma (CODIF) measurements for event 18 December 2011. (a) proton velocity, (b) proton density, OMNI solar wind density, WHISPER electron density, (c) proton parallel and perpendicular temperature, (d) magnetic field magnitude and OMNI IMF magnitude, (e,f) proton spectrograms for the sunward and dawnward looking sectors.

C2 location (not shown here), the spacecraft separation is more than 11000 km, while the separation along the model normal is much smaller, just about 100 km. The estimated shock speed is 1.5–2.2 km/s (comparing the pairs C3-C2 and C4-C2), corresponding to the ramp width about 50 km. However this estimate is very unreliable, since it would strongly depend on small variations of the actual normal.

5   The full resolution waveform is in Figure 10. Similar to Event 1, there is a dominating oscillation with the frequency about 0.4–0.5 Hz, as well as the lower amplitude waves with the frequency above 1 Hz (Fig. S2). The specific feature of this event is a strong difference of C3 and C4 variations during the first 20 s downstream the front (16:01:25–16:01:35 UT), despite relatively small separation. The substantial difference in waveforms remains also further downstream. This is true also for all other shocks registered during this day (8 crossings within 2 hours in Table S1).

10   Despite these differences, it is possible to perform multipoint separation analysis for the interval 16:01:15-16:01:25 UT, where two waveforms in B_y component (Fig. 10b) are more similar and shifted by a fraction of period. All wave parameters (filtered in the range 0.1–2 Hz) are in Table 2. As in Event 1, the maximum variance eigenvector is almost along Y, the medium
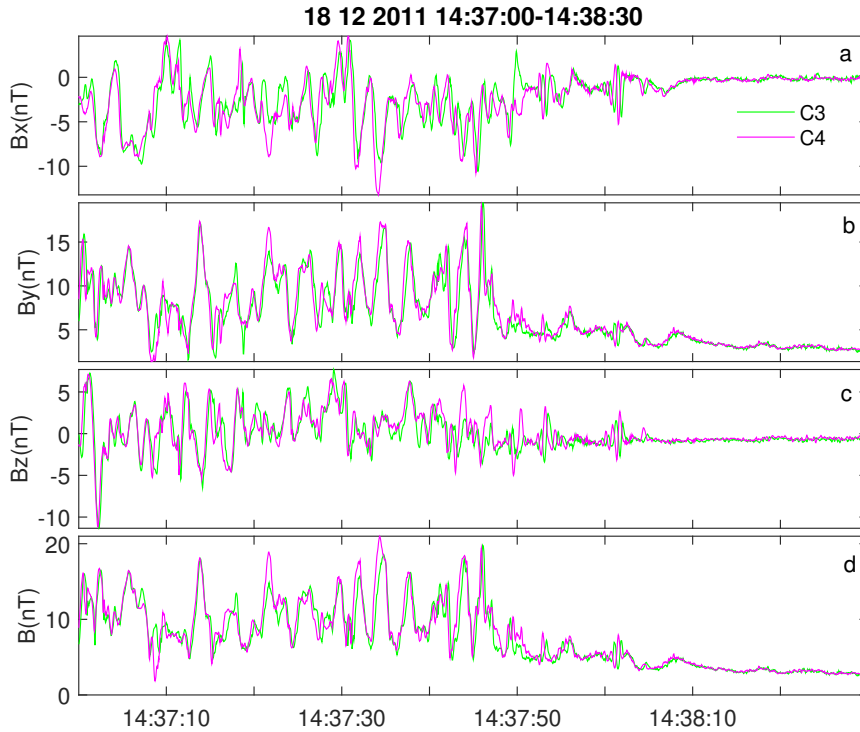
Figure 7. Full resolution magnetic waveform for shock 18 December 2011. In panels (a-d) are components and total value of magnetic field.

eigenvector — along X. Ratios of eigenvalues are $\lambda_{min}/\lambda_{int} = 0.15$, $\lambda_{int}/\lambda_{max} \approx 0.5$, thus the minimum variance (nominal propagation) direction is well defined. The time shift between the magnetic measurements along the maximum variance component is 0.22 s (determined with correlation analysis), while the spacecraft separation along the minimum variance direction is 6.8 km. The resulting wavelength estimate is 61 km for the peak frequency 0.5 Hz. This value is close to the spacecraft
5 separation distance (about 40 km) and thus is generally consistent with the observed substantial difference between magnetic fields at C3 and C4.

The hodograph of magnetic field rotation (Fig. 11), however, shows absence of any stable polarization. It can be interpreted as linear for couple of periods, then almost circular for some periods (most clear in a first panel with the max and middle variance vectors). The coplanarity approach again can not be used here to confirm the wavevector direction, since the angle
10 between the maximum variance direction and the local magnetic field is rather small (20°). The maximum possible wavelength (if the spacecraft separation along the wavevector is maximal 40 km) is $\sim$400 km.
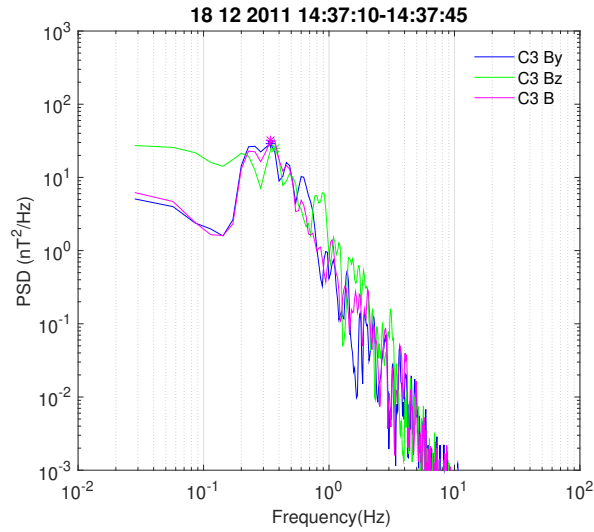
Figure 8. C3 frequency spectra for B_y, B_z components and magnetic field magnitude for shock 18 December 2011.

Table 1. Wave analysis data for shock 18 December 2011, 14:37:27–14:37:47.

max eigenvector, V_{max}	-0.23, 0.94, 0.27
med eigenvector, V_{med}	0.97, 0.20, 0.15
min eigenvector, V_{min}	-0.08, -0.29, 0.95
eigenvalues	2.23, 6.64, 11.50
magnetic field C3, B_3 (nT)	-3.58, 9.53, 0.96
local proton velocity C4 (km/s)	-118.1, 82.1, -29.29
angle, V_{max} and IMF	34°
angle, V_{min} and IMF	110°
angle, V_{max} and B_3	12°
angle, V_{min} and B_3	99°
peak frequency in max component	0.3 Hz
time shift in magnetic field along V_{max}	0.13 s
separation along V_{min}	10 km
wavelength	252 km

3.3 Event 3

One more example is from January 3rd, 2008 (14:30–1435 UT) with Cluster separation $\sim$100 km (Table S1, Fig. S3 in Supplement). OMNI data showed very low IMF (1.1 nT) and $\beta = 39$. Solar wind speed is small $\sim$321 km/s, Alfvén Mach
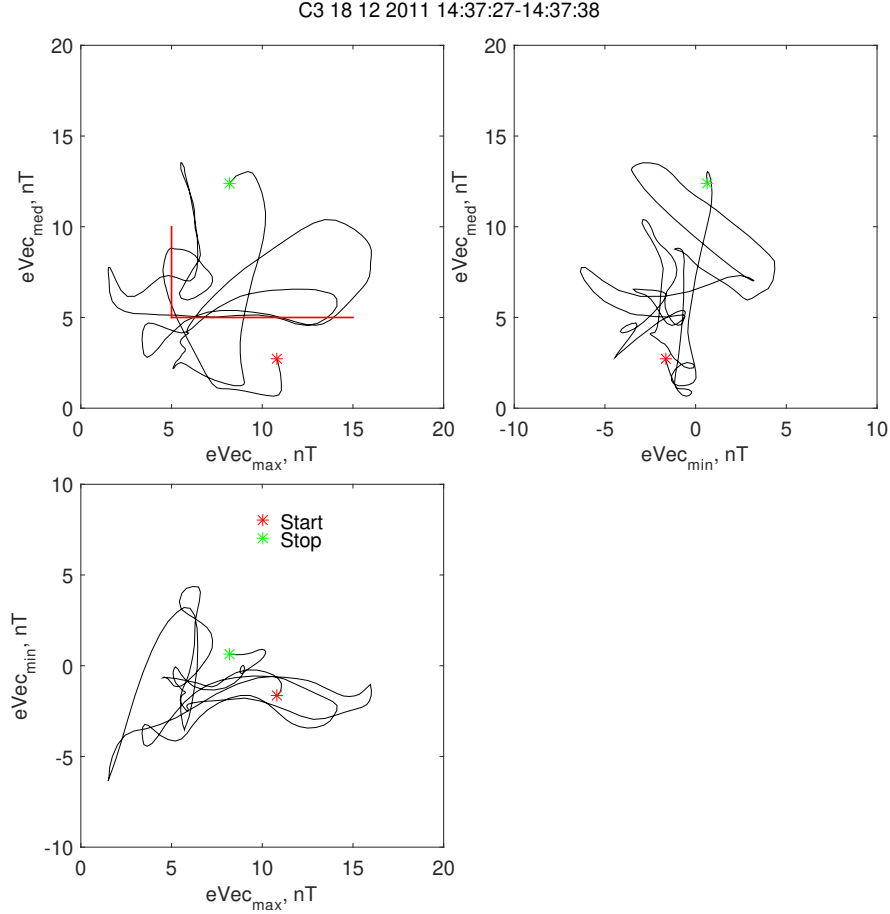
Figure 9. Hodographs of C3 magnetic field in eigenvector coordinates for shock 18 December 2011. Two variants of linear polarization are highlighted by red lines in the first panel.

number is ≈ 42, magnetosonic Mach number is ≈ 7. The model θ_{Bn} is 47°. In Fig. 12 we present local magnetic field along with OMNI data. Though local upstream magnitude is approximately equal to that in OMNI (except starting from 14:30 UT closer to the shock), the upstream field direction changes by more than 90° and the local model θ_{Bn} also changes to more perpendicular geometry. The presence of an earlier shock crossing at 14:20 UT may also affect observed upstream conditions.

5 Strong changes of magnetic field direction on a scale of a minute are also present downstream the shock (Fig.12, right side). Therefore for this shock reliable determination of magnetic geometry is impossible.

Fig. S3 contains overview of magnetic field and plasma parameters. The transition lasts about 2.5 minutes 14:32:00–14:34:30 UT from the first sign of ion velocity change, upstream high-energy ions, growth of parallel ion temperature (Fig. S3e,f) to the stable downstream conditions. The jump in magnetic field magnitude is smeared over about half a minute 14:34:00–14:34:30
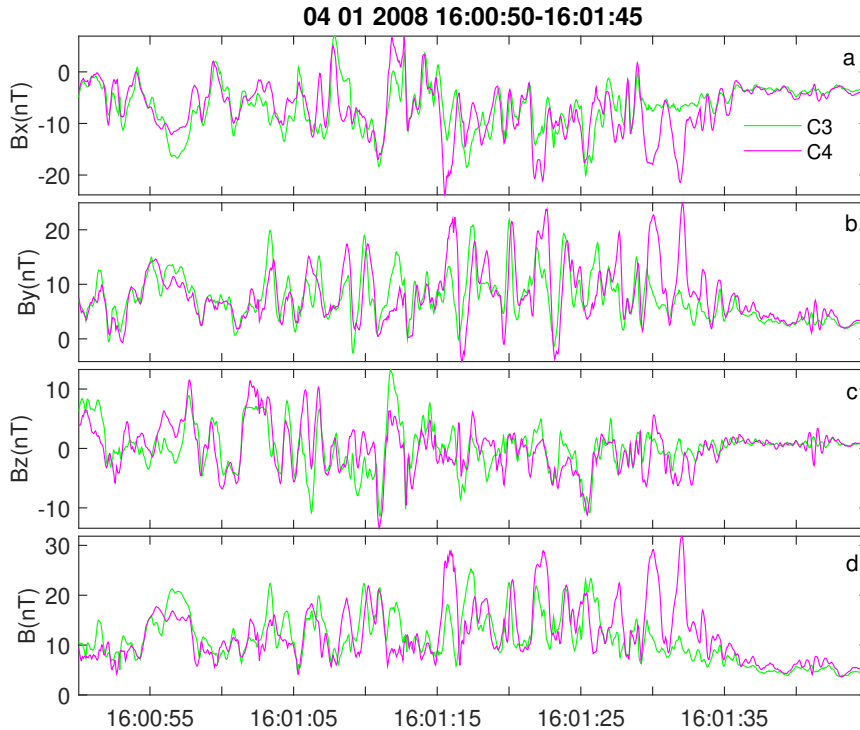
Figure 10. Full resolution magnetic waveform for shock 04 January 2008. In panels (a-d) are components and total value of magnetic field

UT, is wavy, and magnetic magnitude downstream is often as small as 1–2 nT. The nominal shock front transition is somewhat arbitrarily placed at 14:34:10 UT (marked by vertical line in Fig.S3). Some increase of variation amplitudes around 14:34:10 UT can be interpreted as a localized intensification or as a result of shock bounce motion. The ion density increase at ramp does not coinside with the magnetic field increase and is lasting longer.

Similar to Example 1, one can estimate shock speed along the normal, comparing with C2 (not shown here). The spacecraft separation is 5700–5800 km, while the separation along the model normal is 1400 km. The estimated shock speed is 11 km/s, corresponding to the ramp width about 330 km. The covective gyroradius of solar wind protons in IMF is about 2400 unitkm, in the downstream magnetic field — 540 km, the proton inertial length in solar wind is 83 km.

The detailed view of magnetic variations is in Fig. 13. Only relatively high frequency oscillations about 2 Hz are present (frequency spectra are in Fig. S4). There are no wave packets with the stable phase. For example, at 14:34:10–14:34:14 UT, X and Z components are in anticorrelation for C3 and C4, while immediately near, at 14:34:08–14:34:10 UT these components are in phase. Therefore, the reliable multipoint analysis for this event is impossible. Magnetic field hodograph plot for 14:34:10–14:34:14 UT is in Fig.14. It confirms unstable (but consistent with the changing linear) polarization. Assuming that C3 and C4 variations are mostly in antiphase (half a period between the spacecraft), one gets the maximal wavelength estimate ∼200 km.
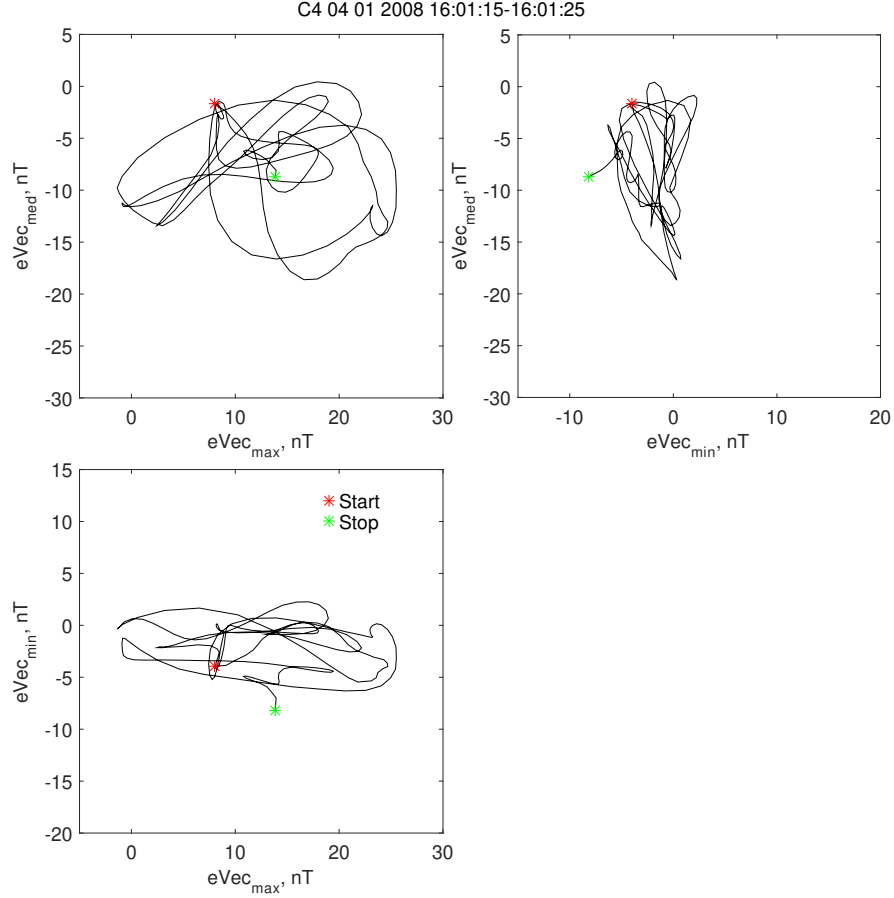
Figure 11. Hodographs of C4 magnetic field in eigenvector coordinates for shock 04 January 2008.

3.4 Observation summary and statistics

Our statistics includes 22 oblique and quasi-perpendicular shocks. The three examples above well illustrate typical shock properties. The minimum θ_{Bn} is 37°, two largest ones are 62° and 83°. Values of β range from 39 to 7.5. All cases are supercritical shocks with magnetosonic Mach number more than 5.5. Alfvén Mach numbers are large because of large β. All shocks exhibit a clear several-minute-long transition zone between pristine solar wind ion flow and magnetosheath. The somewhat smeared main magnetic field and density increase lasts about several tens sec long or several hundred km. This magnetic profile is typical for all our shocks irrespective of θ_{Bn} angle.

Table 2. Wave analysis data for shock 04 January 2008, 16:01:15–16:01:25.

max eigenvector, V_{max}	-0.46 0.87 0.17
med eigenvector, V_{med}	0.88 0.42 0.22
min eigenvector, V_{min}	-0.12 -0.25 0.96
eigenvalues	3.4, 22.9, 45.3
magnetic field C3, B_3 (nT)	-9.05, 9.85, -0.75
local proton velocity C4 (km/s)	-178.3, 125.7, -67.4
angle, V_{max} and IMF	46°
angle, V_{min} and IMF	79°
angle, V_{max} and B_3	20°
angle, V_{min} and B_3	99°
peak frequency in max component	0.5 Hz
time shift in magnetic field along V_{max}	0.22 s
separation along V_{min}	6.8 km
wavelength	61 km

On a smaller time scale of seconds, the magnetic profile is dominated by magnetic variations much larger than the background field, which gradually grow across the magnetic ramp towards downstream. As a result, the exact location of the 'main' magnetic jump can not be defined.

The three examples show characteristics of the dominating magnetic variations, typical for all considered events. The detailed multipoint variation analysis allowed us to obtain the following new information. In most of the shocks (and in Examples 1 and 2) the variations exhibit the well-defined frequency peak $\sim$0.2–0.5 Hz. The phase of these variations is irregular, with no clear persistent polarization. It can be also interpreted as a linear polarization with the frequently changing main direction. However, since the amplitude of variations is larger than the background field, the main axis of linear polarization is always almost along the field vector. Such polarization does not allow us to determine reliably the wave propagation direction and the wavelength. We get the estimates only in the range between several tens and several hundreds km.

Two shock events (Dec. 31, 2003 and our Example 3, Jan. 3, 2008 14:32 UT) have dominating $\sim$2 Hz variations, visually with the more harmonic waveform, but also with the unstable phase. The spatial scale of these variations is smaller than the spacecraft separation, so that it proved to be impossible to determine it with multipoint data. These two shocks are similar to the other events in terms of their other general parameters. Moreover, one of them (Event 3 above) is registered just 10 min after a crossing, which exhibited the first type of variations.
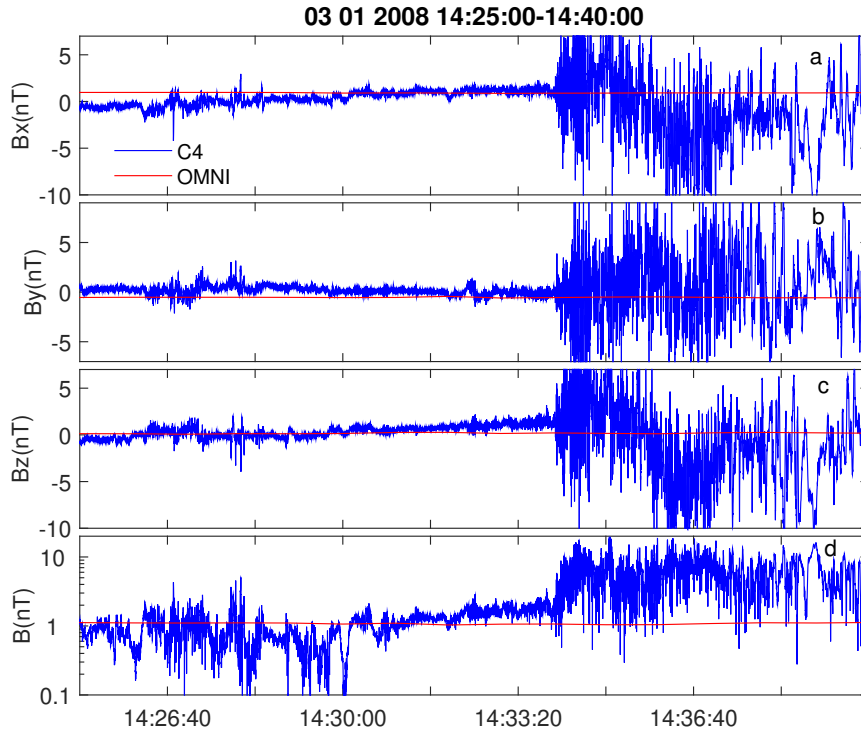
Figure 12. Local upstream and OMNI magnetic field for shock 03 January 2008. In panels (a-d) are components and total value of magnetic field

4 Discussion

4.1 Reliability of solar wind input

High-β solar wind is relatively rare at the Earth orbit. In our study we accepted a somewhat ad-hoc threshold of high β equal to 10. Such interplanetary conditions tend to occur during solar minima, being created by slow cold dense solar wind with low

5 IMF (1–2 nT). However, is not always easy to confirm that the observed shock crossing actually occurred in high-β solar wind interval, identified in OMNI. The first set of problems is related with association of particular crossings with stable high β. These problems are relatively straightforward to identify in data. A more substantial problem is related with the inherent solar wind and IMF variability. We measure solar wind in L1 halo orbit, 1.5 million kilometers away from Earth and with halo radius not less than 200 000 km (for ACE spacecraft). A substantial part of modern OMNI data are taken from Wind spacecraft, which

10 is currently on a much wider halo orbit (300–400 thousand km) (Podladchikova et al., 2018). Solar wind and IMF structures at L1 are not necessarily the same as these that actually affect the magnetosphere. The most questionable is spatial persistence of relatively small changes of IMF from 2 to 1 nT, required for creation of very high-β intervals.
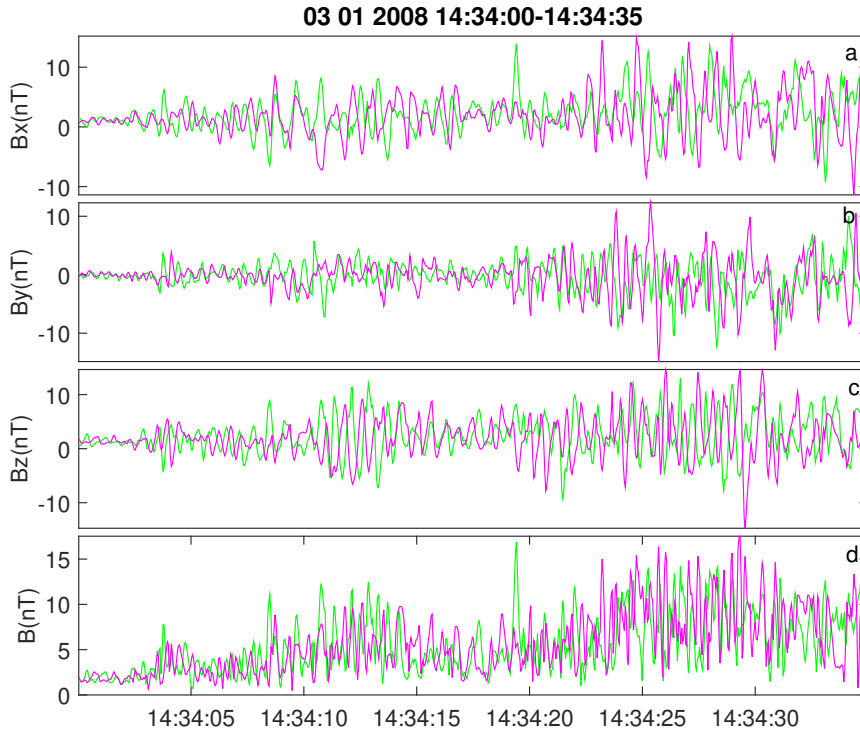
Figure 13. Full resolution magnetic waveform for shock 03 January 2008. In panels (a-d) are components and total value of magnetic field, colors are like in Figs. 7 and 10.

Though the specific analysis of the spatial scales of high-β areas in solar wind was not performed, available reports indicate significant potential problems. The ISEE data study suggested that during periods of medium to low variance of magnetic field, magnetic features with the scales about 20 R_E perpendicular to IMF may occur (Crooker et al., 1982). Comparison of L1 Wind and near-Earth Interball data for 1996–1999 (Petrukovich et al., 2001) have shown, that IMF structures, associated
5 with geomagnetic storms (with the threshold of IMF B_z GSM below –10 nT during 3 hours) are practically the same in L1 and the near-Earth orbits. However, about 20–80% of the smaller everyday IMF variations, causing substorms (several nT in magnitude on one-hour scale) are different by more than 25%.

Thus very high β values in OMNI are not readily applicable for a shock study. It is not always possible to check solar wind β immediately before shock crossing. A spacecraft needs to probe pristine solar wind and then rapidly cross the shock,
10 or there should be an additional near-Earth solar wind monitor. Magnetic field can be reliably measured with magnetometer (still assuming an offset uncertainty of about 0.1 nT). Comparison of ion density and temperature measurements is more problematic. Assumptions on the constant helium content and constant electron temperature, used while OMNI β calculations, may also result in some errors. For example, a factor of two change in electron temperature will result in the change of β by
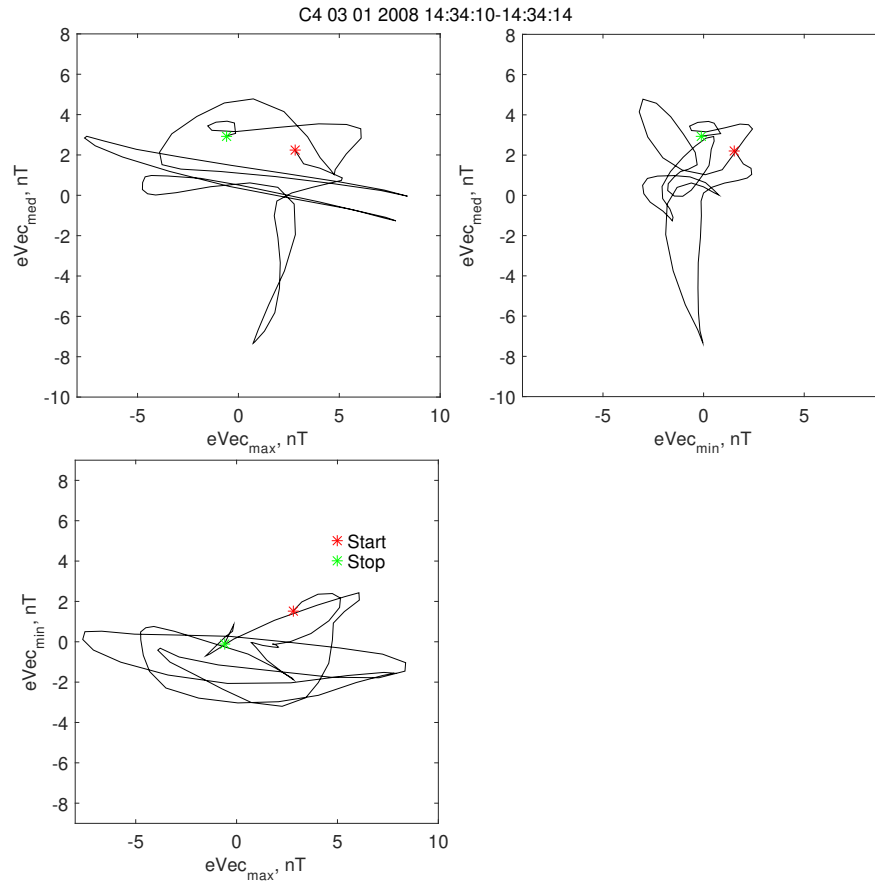
Figure 14. Hodographs of C4 magnetic field in eigenvector coordinates for shock 03 January 2008 for 14:34:10-14:34:14.

about 30%. A factor of two variations of the He++ content will result in variations of β around 10%. Of course, an additional (relative to those found in the OMNI set) high β intervals may actually form near the bow shock, as a side product of such variability.

4.2 General shock properties

5 Relatively compact large-scale structure of the observed shock transitions (about couple of minutes) is similar to that reported for oblique and quasi perpendicular shocks. It is distinctly different from the structure of quasi-parallel shocks, which are extended up to several Earth radii (Burgess et al., 2005).

The apparent increased width of the magnetic jump in our cases ($\sim$30 s) might be related with the larger ion gyro radius in the high-β plasma and relatively slow shock motion (only about 10 km/s). In fact, for Event 1 and Event 3, where it was

10 possible to estimate the spatial scale, the ramp length (divided by 2) was about 0.5 of convective proton gyroradius in the downstream field and about 2-3 time larger, than ion inertial length in the solar wind, consistent with the statistics of Bale et al. (2003).

Magnetic variations during this ramp-like increase have the amplitude comparable or larger than the background magnetic field, so that there is no 'stable' magnetic structure on the time scales of seconds. In comparison, for a supercritical quasi-

15 perpendicular low-β shock, one usually defines, starting from the upstream, the prolonged interval of somewhat enhanced density and magnetic field (shock foot, lasting tens of seconds) and the sharp main increase (ramp, lasting seconds). The ramp is often used to determine the shock motion with multipoint measurements, but in our case it is impossible.

A more detailed phenomenological description of this shock transition requires analysis of ion kinetics, which will be performed elsewhere. Possible dependence of shock spatial scale on β is an interesting aspect and should be addressed in

20 future studies on larger statistics.

4.3 Magnetic variation properties

Observations of the high-amplitude magnetic variations and absence of a sharp ramp profile in high-β events are similar to those earlier presented by Formisano et al. (1975); Farris et al. (1992) (as far as it can be discerned with visual examination of figures). In this invesigation we improved our knowledge, analyzing spectral and polarization properties of these variations.

25 With two Cluster spacecraft separated by several tens km it was possible to estimate the spatial scale of these dominating variations. Three typical variants were found. In some events (Example 1) variations had rather irregular form, typical frequency of about 0.5 Hz, and were very similar on the two spacecraft, suggesting the scale of some hundred km. The second variant of a spatial scale is illustrated with Example 2. It includes the variations visually similar to that in Example 1, but with a mix of scales of the order of hundred km, which can be captured with our spacecraft separation, and of the order of tens km. As

30 a result, the waveforms are rather different, but common features can sometimes be traced. Finally, the third variant (Example 3) contains more harmonic waves with higher frequencies around 1–2 Hz and the quantitatively unresolved dominating spatial scale of at most 200 km.

The observed variations are very different from that in low-β supercritical events (e.g. Krasnoselskikh et al., 2013), where clear whistler wave packets with elliptic polarization dominate. Observed polarization is also not consistent with the Alfvén mode, earlier suggested for high-β shock (Coroniti, 1970; Kennel and Sagdeev, 1967).

The wavelength can be determined independently to propagation direction only with four measuring points. Alternatively one can fix propagation direction with the minimum variance analysis in the case of elliptic polarization or with the coplanarity supposition. Unfortunately, in our cases it proved impossible to determine the wavevector direction reliably by either methods, since we have linearly polarized waves with maximum variance direction along the main magnetic field. Note, that such configuration is inevitable for a variation much larger than the background field.

Linear polarization with very high amplitude, substantially changing the total magnetic field, suggests strong non-linearity and compressive nature. Absence of any several-periods-long wave packets with the stable phase also suggests strong spatial localisation.

Dominating wave mode downstream of the shock front was also addressed in a number of other investigations, however cases of really high $\beta > 10$ were not specifically addressed. Hubert et al. (1989) identified the mirror waves, comparing magnetic field with density, provided by the fast electron measurements of ISEE project. Balikhin et al. (1997) identified the intermediate mode with two-point AMPTE data analysis. Lacombe et al. (1992) suggested for higher-β shocks the mirror mode with linear polarization, and successfully used coplanarity assumption to define the wavevector direction. Czaykowska et al. (2001) have shown compressive mode as well as left-hand polarized mode in shocks with $\beta > 1$. Therefore, almost full variety of possible wave mode variants was identified.

A definite plasma mode analysis critically depends on reliable determination of the wave propagation (wavevector) direction, which proved to be impossible in our cases. Also, it should be noted, that all studies referenced above, used several-minute data intervals, which were often several minutes away from the shock transition, with the natural motivation to access the long sets of uniform variations. In the most of cases, the analysed frequencies were below 0.1 Hz. This approach is different from ours, in which we addressed relatively short intervals of the most powerful oscillations.

An alternative wave mode candidate, frequently suggested for high-β plasma, is the Weibel instability, which is fundamentally similar to drift mirror mode. With no seed magnetic field the Weibel mode has only imaginary frequency, magnetic field variations are growing faster, than propagate. For a finite magnetic field, Pokhotelov and Balikhin (2012) suggested that the Weibel mode grows as a mix of two opposite circular polarizations, attains some small real part of frequency. Thus in some features (linear polarization, chaotic phase) it is consistent with our observations.

An important aspect is quite possible instability of the shock front, exhibiting itself as cyclic growth of a coherent ramp structure, subsequently decaying with large-scale magnetic variations (e.g., Lefebvre et al., 2009). Less coherent shock structure in Event 3 may be explained with such an effect, but more statistics is necessary to confirm such hypothesis.

5 Conclusions

High-β ($\beta > 10$) shocks are relatively rare and largely unexplored class of Earth bow shock. Formation of high-β interplanetary plasmas is mostly related with dense slow solar wind and very low magnetic field up to 1–2 nT. Due to spatial variability of low IMF, it is difficult to determine shock geometry for higher β (in OMNI) cases. Generally speaking, at some very large β (very low magnetic field) shock structure should become independent from magnetic field direction. This is an interesting direction of future studies.

Dominating magnetic variations have amplitudes much larger than the background field, frequencies 0.2–0.5 Hz, sometimes, $\sim$2 Hz. Polarization is mostly irregular and close to linear, the spatial scales range from several tens to couple hundred km. These properties are definitely inconsistent with the elliptically polarized fast magnetosonic or Alfvén modes earlier reported for other shock types. In some features the variations may be consistent with the Weibel instability, but observations with more closely spaced spacecraft are necessary to conclude more definitely on the wave mode.

Author contributions. OMC and PIS performed the data processing and analysis. AAP is responsible for data analysis and interpretation. AAP prepared the manuscript with contributions from all co-authors.

Competing interests. The authors declare that they have no conflict of interest.

Acknowledgements. The data analysis was supported with Russian Science Fund projects 05-14-00824 and 19-12-00313. We are thankful for Cluster Science Archive, CDAWeb and OMNI for availability of spacecraft data.

References

Axford, W. I., Leer, E., and Skadron, G.: The Acceleration of Cosmic Rays by Shock Waves, International Cosmic Ray Conference, 11, 132, 1977.

Bale, S. D., Mozer, F. S., and Horbury, T. S.: Density-Transition Scale at Quasiperpendicular Collisionless Shocks, Physical Review Letters, 91, 265004, https://doi.org/10.1103/PhysRevLett.91.265004, 2003.

Balikhin, M., Gedalin, M., and Petrukovich, A.: New mechanism for electron heating in shocks., , 70, 1259–1262, https://doi.org/10.1103/PhysRevLett.70.1259, 1993.

Balikhin, M. A., Woolliscroft, L. J. C., Alleyne, H. S. C., Dunlop, M., and Gedalin, M. A.: Determination of the dispersion of low frequency waves downstream of a quasiperpendicular collisionless shock, Annales Geophysicae, 15, 143–151, https://doi.org/10.1007/s00585-997-0143-x, 1997.

Balogh, A., Carr, C. M., Acuña, M. H., Dunlop, M. W., Beek, T. J., Brown, P., Fornaçon, K. H., Georgescu, E., Glassmeier, K. H., Harris, J., Musmann, G., Oddy, T., and Schwingenschuh, K.: The Cluster Magnetic Field Investigation: overview of in-flight performance and initial results, Annales Geophysicae, 19, 1207–1217, https://doi.org/10.5194/angeo-19-1207-2001, 2001.

Burgess, D., Lucek, E. A., Scholer, M., Bale, S. D., Balikhin, M. A., Balogh, A., Horbury, T. S., Krasnoselskikh, V. V., Kucharek, H., Lembège, B., Möbius, E., Schwartz, S. J., Thomsen, M. F., and Walker, S. N.: Quasi-parallel Shock Structure and Processes, , 118, 205–222, https://doi.org/10.1007/s11214-005-3832-3, 2005.

Coroniti, F. V.: Turbulence structure of high-β perpendicular fast shocks, Journal of Geophysical Research, 75, 7007, https://doi.org/10.1029/JA075i034p07007, 1970.

Crooker, N. U., Siscoe, G. L., Russell, C. T., and Smith, E. J.: Factors controlling degree of correlation between ISEE 1 and ISEE 3 interplanetary magnetic field measurements, Journal of Geophysical Research, 87, 2224–2230, https://doi.org/10.1029/JA087iA04p02224, 1982.

Czaykowska, A., Bauer, T. M., Treumann, R. A., and Baumjohann, W.: Magnetic field fluctuations across the Earth's bow shock, Annales Geophysicae, 19, 275–287, https://doi.org/10.5194/angeo-19-275-2001, 2001.

Décréau, P. M. E., Fergeau, P., Krasnoselskikh, V., Le Guirriec, E., Lévêque, M., Martin, P., Randriamboarison, O., Rauch, J. L., Sené, F. X., Séran, H. C., Trotignon, J. G., Canu, P., Cornilleau, N., de Féraudy, H., Alleyne, H., Yearby, K., Mögensen, P. B., Gustafsson, G., André, M., Gurnett, D. C., Darrouzet, F., Lemaire, J., Harvey, C. C., Travnicek, P., and Whisper Experimenters Group: Early results from the Whisper instrument on Cluster: an overview, Annales Geophysicae, 19, 1241–1258, https://doi.org/10.5194/angeo-19-1241-2001, 2001.

Dimmock, A. P., Balikhin, M. A., Walker, S. N., and Pope, S. A.: Dispersion of low frequency plasma waves upstream of the quasi-perpendicular terrestrial bow shock, Annales Geophysicae, 31, 1387–1395, https://doi.org/10.5194/angeo-31-1387-2013, 2013.

Donnert, J., Vazza, F., Brüggen, M., and ZuHone, J.: Magnetic Field Amplification in Galaxy Clusters and Its Simulation, , 214, 122, https://doi.org/10.1007/s11214-018-0556-8, 2018.

Farris, M. H., Petrinec, S. M., and Russell, C. T.: The thickness of the magnetosheath: Constraints on the polytropic index, Geophysical Research Letters, 18, 1821–1824, https://doi.org/10.1029/91GL02090, 1991.

Farris, M. H., Russell, C. T., Thomsen, M. F., and Gosling, J. T.: ISEE 1 and 2 observations of the high beta shock, Journal of Geophysical Research, 97, 19 121–19 127, https://doi.org/10.1029/92JA01976, 1992.

Formisano, V., Russell, C. T., Means, J. D., Greenstadt, E. W., Scarf, F. L., and Neugebauer, M.: Collisionless shock waves in space: A very high β structure, Journal of Geophysical Research, 80, 2013, https://doi.org/10.1029/JA080i016p02013, 1975.

Hobara, Y., Balikhin, M., Krasnoselskikh, V., Gedalin, M., and Yamagishi, H.: Statistical study of the quasi-perpendicular shock ramp widths, Journal of Geophysical Research (Space Physics), 115, A11106, https://doi.org/10.1029/2010JA015659, 2010.

Hubert, D., Perche, C., Harvey, C. C., Lacombe, C., and Russell, C. T.: Observation of mirror waves downstream of a quasi-perpendicular shock, Geophysical Research Letters, 16, 159–162, https://doi.org/10.1029/GL016i002p00159, 1989.

5 Hubert, D., Lacombe, C., Harvey, C. C., Moncuquet, M., Russell, C. T., and Thomsen, M. F.: Nature, properties, and origin of low-frequency waves from an oblique shock to the inner magnetosheath, Journal of Geophysical Research, 103, 26 783–26 798, https://doi.org/10.1029/98JA01011, 1998.

Kennel, C. F. and Sagdeev, R. Z.: Collisionless shock waves in high β plasmas: 1, Journal of Geophysical Research, 72, 3303–3326, https://doi.org/10.1029/JZ072i013p03303, 1967.

10 Kennel, C. F., Edmiston, J. P., and Hada, T.: A quarter century of collisionless shock research, Washington DC American Geophysical Union Geophysical Monograph Series, 34, 1–36, https://doi.org/10.1029/GM034p0001, 1985.

Krasnoselskikh, V., Balikhin, M., Walker, S. N., Schwartz, S., Sundkvist, D., Lobzin, V., Gedalin, M., Bale, S. D., Mozer, F., Soucek, J., Hobara, Y., and Comisel, H.: The Dynamic Quasiperpendicular Shock: Cluster Discoveries, , 178, 535–598, https://doi.org/10.1007/s11214-013-9972-y, 2013.

15 Krasnoselskikh, V. V., Lembège, B., Savoini, P., and Lobzin, V. V.: Nonstationarity of strong collisionless quasiperpendicular shocks: Theory and full particle numerical simulations, Physics of Plasmas, 9, 1192–1209, https://doi.org/10.1063/1.1457465, 2002.

Krymskii, G. F.: A regular mechanism for the acceleration of charged particles on the front of a shock wave, Soviet Physics Doklady, 22, 327, 1977.

Lacombe, C., Pantellini, F. G. E., Hubert, D., Harvey, C. C., Mangeney, A., Belmont, G., and Russell, C. T.: Mirror and Alfvenic waves
20   observed by ISEE 1-2 during crossings of the earth's bow shock, Annales Geophysicae, 10, 772–784, 1992.

Lefebvre, B., Seki, Y., Schwartz, S. J., Mazelle, C., and Lucek, E. A.: Reformation of an oblique shock observed by Cluster, Journal of Geophysical Research (Space Physics), 114, A11107, https://doi.org/10.1029/2009JA014268, 2009.

Markevitch, M. and Vikhlinin, A.: Shocks and cold fronts in galaxy clusters, , 443, 1–53, https://doi.org/10.1016/j.physrep.2007.01.001, 2007.

25 Petrukovich, A. A., Romanov, S. A., and Klimov, S. L.: Direct Measurements of AC Plasma Currents in the Outer Magnetosphere, Washington DC American Geophysical Union Geophysical Monograph Series, 103, 199, https://doi.org/10.1029/GM103p0199, 1998.

Petrukovich, A. A., Klimov, S. I., Lazarus, A., and Lepping, R. P.: Comparison of the solar wind energy input to the magnetosphere measured by Wind and Interball-1, Journal of Atmospheric and Solar-Terrestrial Physics, 63, 1643–1647, https://doi.org/10.1016/S1364-6826(01)00039-6, 2001.

30 Podladchikova, T., Petrukovich, A., and Yermolaev, Y.: Geomagnetic storm forecasting service StormFocus: 5 years online, Journal of Space Weather and Space Climate, 8, A22, https://doi.org/10.1051/swsc/2018017, 2018.

Pokhotelov, O. A. and Balikhin, M. A.: Weibel instability in a plasma with nonzero external magnetic field, Annales Geophysicae, 30, 1051–1054, https://doi.org/10.5194/angeo-30-1051-2012, 2012.

Rème, H., Aoustin, C., Bosqued, J. M., Dandouras, I., Lavraud, B., Sauvaud, J. A., Barthe, A., Bouyssou, J., Camus, T., Coeur-Joly, O.,
35   Cros, A., Cuvilo, J., Ducay, F., Garbarowitz, Y., Medale, J. L., Penou, E., Perrier, H., Romefort, D., Rouzaud, J., Vallat, C., Alcaydé, D., Jacquey, C., Mazelle, C., D'Uston, C., Möbius, E., Kistler, L. M., Crocker, K., Granoff, M., Mouikis, C., Popecki, M., Vosbury, M., Klecker, B., Hovestadt, D., Kucharek, H., Kuenneth, E., Paschmann, G., Scholer, M., Sckopke, N., Seidenschwang, E., Carlson, C. W., Curtis, D. W., Ingraham, C., Lin, R. P., McFadden, J. P., Parks, G. K., Phan, T., Formisano, V., Amata, E., Bavassano- Cattaneo, M. B.,

Baldetti, P., Bruno, R., Chionchio, G., di Lellis, A., Marcucci, M. F., Pallocchia, G., Korth, A., Daly, P. W., Graeve, B., Rosenbauer, H., Vasyliunas, V., McCarthy, M., Wilber, M., Eliasson, L., Lundin, R., Olsen, S., Shelley, E. G., Fuselier, S., Ghielmetti, A. G., Lennartsson, W., Escoubet, C. P., Balsiger, H., Friedel, R., Cao, J. B., Kovrazhkin, R. A., Papamastorakis, I., Pellat, R., Scudder, J., and Sonnerup, B.: First multispacecraft ion measurements in and near the Earth's magnetosphere with the identical Cluster ion spectrometry (CIS) experiment, Annales Geophysicae, 19, 1303–1354, https://doi.org/10.5194/angeo-19-1303-2001, 2001.

5   Sagdeev, R. Z.: Cooperative Phenomena and Shock Waves in Collisionless Plasmas, Reviews of Plasma Physics, 4, 23, 1966.

Schwartz, S. J., Henley, E., Mitchell, J., and Krasnoselskikh, V.: Electron Temperature Gradient Scale at Collisionless Shocks, , 107, 215002, https://doi.org/10.1103/PhysRevLett.107.215002, 2011.

Scudder, J. D., Mangeney, A., Lacombe, C., Harvey, C. C., Aggson, T. L., Anderson, R. R., Gosling, J. T., Paschmann, G., and Russell, C. T.:

10   The resolved layer of a collisionless, high β, supercritical, quasi-perpendicular shock wave 1. Rankine- Hugoniot geometry, currents, and stationarity, Journal of Geophysical Research, 91, 11 019–11 052, https://doi.org/10.1029/JA091iA10p11019, 1986.

Vasko, I. Y., Mozer, F. S., Krasnoselskikh, V. V., Artemyev, A. V., Agapitov, O. V., Bale, S. D., Avanov, L., Ergun, R., Giles, B., Lindqvist, P. A., Russell, C. T., Strangeway, R., and Torbert, R.: Solitary Waves Across Supercritical Quasi-Perpendicular Shocks, Geophysical Research Letters, 45, 5809–5817, https://doi.org/10.1029/2018GL077835, 2018.

15   Walker, S., Alleyne, H., Balikhin, M., André, M., and Horbury, T.: Electric field scales at quasi-perpendicular shocks, Annales Geophysicae, 22, 2291–2300, https://doi.org/10.5194/angeo-22-2291-2004, 2004.

Wilson, Lynn B., I., Stevens, M. L., Kasper, J. C., Klein, K. G., Maruca, B. A., Bale, S. D., Bowen, T. A., Pulupa, M. P., and Salem, C. S.: The Statistical Properties of Solar Wind Temperature Parameters Near 1 au, The Astrophysical Journal Supplement Series, 236, 41, https://doi.org/10.3847/1538-4365/aab71c, 2018.

20   Winterhalter, D. and Kivelson, M. G.: Observations of the Earth's bow shock under high Mach number/high plasma beta solar wind conditions, Geophysical Research Letters, 15, 1161–1164, https://doi.org/10.1029/GL015i010p01161, 1988.